Title

Distributed hydrological modelling in California semi-arid shrublands: MIKE SHE model calibration and uncertainty estimation

Journal

Journal of Hydrology, 317(3-4)

ISSN

0022-1694

Authors

McMichael, Christine E

Hope, Allen S

Loaiciga, Hugo A

Publication Date

2006-02-01

DOI

10.1016/j.jhydrol.2005.05.023

Peer reviewed

Available online at www.sciencedirect.com
SCIENCE DIRECT®
Journal of Hydrology 317 (2006) 307–324
Journal of Hydrology
www.elsevier.com/locate/jhydrol

Distributed hydrological modelling in California semi-arid shrublands: MIKE SHE model calibration and uncertainty estimation

Christine E. McMichael[a,*], Allen S. Hope[b,1], Hugo A. Loaiciga[c,2]

[a]Institute for Regional Analysis and Public Policy, Morehead State University, Morehead, Kentucky, USA
[b]Department of Geography, San Diego State University, San Diego, California, USA
[c]Department of Geography, University of California-Santa Barbara, Santa Barbara, California, USA

Received 18 August 2004; revised 31 March 2005; accepted 20 May 2005

Abstract

The Generalized Likelihood Uncertainty Estimation (GLUE) methodology is used for model calibration, testing and predictive uncertainty estimation in the application of the MIKE SHE hydrologic model for estimating monthly streamflow in a semi-arid shrubland (chaparral) catchment in central California. Monte Carlo simulation is used to randomly generate one thousand parameter sets for a 20-year calibration period encompassing variable climatic and wildfire conditions, from which behavioural (acceptable) MIKE SHE parameter sets are identified and 5% and 95% uncertainty bounds for monthly streamflow are calculated. This group of behavioural parameter sets is subsequently used to predict streamflow and to construct uncertainty bounds for a 12-year test period with climatic and fire characteristics different from those of the calibration period. More than two-thirds of the observations in each period fell within the corresponding uncertainty bounds, suggesting a similar level of model performance in the calibration and test periods. Prediction errors (i.e. observations falling outside the uncertainty bounds) were generally associated with large rainfall and wildfire events and are indicative of deficiencies in model structure, uncertainty in input data, and/or errors in observed streamflow. The effect of uncertainty in remote sensing-based LAI model inputs on the uncertainty associated with MIKE SHE streamflow predictions receives special attention in this work due to the fire-prone nature of the study area and the increasing use of remotely sensed LAI estimates in distributed hydrological modelling applications. Results from MIKE SHE simulations for seven LAI input scenarios (including the baseline LAI sequence used in the model calibration and testing phase of this study) indicate that differences in predictive uncertainty between scenarios are usually less than $\pm 10\%$. This is evidence that the baseline LAI trajectory is generally appropriate for distributed hydrological modelling of chaparral catchments.

Keywords: Generalised likelihood uncertainty estimation; Hydrologic uncertainty; Leaf area index; MIKE SHE

1. Introduction and research objectives

Wildfires in California semi-arid shrublands (i.e. chaparral) dramatically alter catchment land cover and initiate a complex sequence of vegetation recovery events spanning several decades. Future climate- and anthropogenic-induced changes may

* Corresponding author. Tel.: +606 783 5442; fax: +606 783 5092.
E-mail addresses: c.mcmichael@moreheadstate.edu (C.E. McMichael), hope1@mail.sdsu.edu (A.S. Hope), hugo@geog.ucsb.edu (H.A. Loaiciga).
[1] Tel.: +619 594 2777; fax: +619 594 4938.
[2] Tel.: +805 893 8053; fax: +805 893 3146.

0022-1694/$ - see front matter © 2005 Elsevier B.V. All rights reserved.
doi:10.1016/j.jhydrol.2005.05.023

modify the current wildfire regime in this region (Ryan, 1991; Davis and Michaelsen, 1995; Lenihan et al., 2003) and, consequently, post-fire vegetation recovery patterns and related streamflow dynamics. Catchment experiments have provided insights into the effects of fire on streamflow in semi-arid shrublands (Hoyt and Troxell, 1932; Scott, 1993; Lavabre et al., 1993; Loaiciga et al., 2001), however extrapolation of these results is constrained by the limited spatial and/or temporal scales examined. It is not feasible to conduct the field experiments required to improve our understanding of the hydrological impacts of fire at the spatial (tens to hundreds of square kilometres) and temporal (seasonal and annual) scales most relevant to California water resource managers. Rather, a distributed hydrological modelling approach is required, one capable of representing changes in vegetation patterns following fire and the concomitant effects on catchment hydrological processes.

The generalised likelihood uncertainty estimation (GLUE, Binley and Beven, 1991; Beven and Binley, 1992) methodology is used in this paper to characterise the uncertainty and error associated with using the distributed MIKE SHE hydrological model to make monthly streamflow predictions for a medium-size chaparral catchment located in central California, USA (see Refsgaard and Storm (1995) for a detailed description of the MIKE SHE model; see Section 2.1 of this paper for a summary description). Specifically, the goal is to investigate the annual and seasonal variation in uncertainty and error associated with streamflow predictions for a range of rainfall and fire conditions in model calibration and test periods.

Information on the spatio-temporal patterns of green leaf area is often required in distributed hydrological models to simulate the impacts of land cover change (e.g. due to fire) on catchment processes. The variable most widely used to represent changes in canopy leaf area in distributed modelling studies is the leaf area index (LAI), the total (one-sided) leaf area per unit ground area. Remote sensing-based techniques have been used to characterise LAI dynamics over large space and time scales for hydrological modelling studies in a variety of environments (e.g. Mackay and Band, 1997; Sandholt et al., 1999; Watson et al., 1999; Anderson et al., 2002). There are advantages in using such techniques. Yet, validation of these values is difficult and not often performed-leading to unknown errors in estimated LAI values. For example, uncertainty in LAI estimates may arise from errors in image processing procedures and/or uncertainties in calibrating LAI models developed using spectral vegetation indices (e.g. the normalised difference vegetation index, NDVI). Despite the widespread use of remote sensing-derived LAI inputs in distributed hydrological models, we have little understanding of how uncertainty in these estimates translates into uncertainty in model predictions (i.e. predictive uncertainty). As will be shown in this paper, sizeable model prediction errors occurred following a very large wildfire in the study catchment. Consequently, following the model calibration and testing phases of this study, the effects of uncertainty in remote sensing-based LAI inputs on model streamflow predictions were examined. The second goal of this paper is to present these results and discuss their implications for distributed hydrological modelling in this environment.

2. Methods

2.1. MIKE SHE modelling system

MIKE SHE is a derivative of the Système Hydrologique Européen, SHE, (Abbott et al., 1986a, b) and is a physically-based, spatially distributed hydrological model that has been widely used to study a variety of water resource and environmental problems under diverse climatological and hydrological regimes (Refsgaard and Storm, 1995). A modified version of MIKE SHE (after Andersen et al., 2001) was used in this study, a decision necessitated by the lack of detailed knowledge and limited data regarding the groundwater environment in the study catchment. The major differences between the original (MIKE SHE) and modified (MSHE_m) versions of the model occur in the representations of flow in the unsaturated and saturated zones. In MIKE SHE vertical flow in the unsaturated zone is modelled using the full Richards equation, whereas in MSHE_m it is calculated using a simplified Richards equation. The soil column within each grid cell is divided into a number of layers, each

with associated parameters based on soil type. Groundwater flow in MIKE SHE is represented by a three-dimensional saturated zone module that is dynamically coupled to the unsaturated zone module. A net vertical drainage from the unsaturated zone is accumulated in a series of linear interflow reservoirs in MSHE_m. The interflow reservoirs model lateral subsurface throughflow using a reservoir threshold parameter and a set of horizontal time constants. A vertical time constant is used to compute drainage from each interflow reservoir to the catchment's groundwater reservoir. Finally, baseflow from this groundwater reservoir is modelled as a function of current storage and a horizontal time constant.

Interception of rainfall in MSHE_m (and MIKE SHE) is computed as a function of the canopy interception storage capacity and the leaf area index (LAI)-a key variable in the study area, where greater than 70% of rainfall is returned to the atmosphere via evapotranspiration (Poole et al., 1981). Evaporation from canopy storage is governed by the potential evapotranspiration rate (PE, a model input; see Section 2.4.1); stem flow occurs once the storage is filled. Three separate, non-linear, functions (f_1, f_2, f_3) control plant transpiration (T): (1) f_1(LAI), (2) f_2(soil volumetric moisture content, θ), and (3) f_3(rooting depth and density); each function can take on a value between zero and one. These functions express the dependence of plant transpiration on the abundance of green leaves, the amount of water available in the root zone, and the distribution of roots with depth, respectively. Transpiration is calculated by successively multiplying PE by the value of each function (after Kristensen and Jensen, 1975). Soil evaporation is calculated as a function of soil moisture in the upper layer of the soil column and is added to T in order to compute actual evapotranspiration (AE) (Refsgaard and Storm, 1995). The reader is referred to Refsgaard and Storm (1995); DHI Water and Environment (2000), and Andersen et al. (2001) for a complete description of the model structure and set up.

2.2. GLUE methodology

Many studies have demonstrated the difficulties that arise in identifying, calibrating and validating physically-based hydrological models. Such difficulties stem from uncertainties in model structure, boundary conditions, and catchment parameterisation, as well as errors in input and observed variables (Freer and Beven, 1996; Zak and Beven, 1999; Brazier et al., 2000; Beven and Freer, 2001; Loaiciga, 2003). Hence, the search for a globally optimal parameter set is neither realistic nor practical in most hydrological modelling applications. The advent of population-based search algorithms (e.g. genetic algorithms and the shuffled complex evolution) has certainly increased the efficiency of model optimization efforts, yet the existence of a single optimal parameter set for a particular model application remains questionable. Even groundwater models with well-defined governing equations that involve physically meaningful parameters (e.g. Loaiciga and Marino, 1987) may utilize measured values as initial parameter estimates which are then refined using methods such as GLUE.

The GLUE methodology (Binley and Beven, 1991; Beven and Binley, 1992) explicitly recognizes the co-existence of alternative parameter sets and models (i.e. equifinality) and provides a suitable framework for model calibration and uncertainty estimation under non-uniqueness. Implementing GLUE requires making Monte Carlo simulations using a large number of parameter sets, assessing the relative performance of each set by comparing model estimates with observed data, and retaining only those parameter sets that provide behavioural (acceptable) predictions. The relative performance of each parameter set is evaluated on the basis of a likelihood measure (or measures) calculated by comparing model predictions with observed data. It should be noted that, in the context of GLUE, the meaning of 'likelihood' is broader than that found in classical statistics (Beven and Binley, 1992). A parameter set is classified as behavioural if the corresponding likelihood value is equal to or greater than a specified threshold value. Parameter sets that do not meet this criterion are rejected as non-behavioural.

The final step in the GLUE procedure is to establish predictive uncertainty bounds for comparison with observed values. First, the set of behavioral likelihood values is rescaled to achieve a cumulative sum of unity by dividing each value by the sum of the likelihood values. Next, behavioural model predictions for each time step are ranked in ascending order and each prediction is assigned to a user-specified bin. The rescaled likelihood values associated with the

ranked predictions in each bin are summed to calculate the height of the corresponding bar in the density plot. A cumulative density plot is constructed by graphing the cumulative sum of the likelihood values versus the ranked model predictions. Typically, the 5th and 95th percentiles calculated at each time step are used to generate the predictive uncertainty bounds over the period of observations (Binley and Beven, 1991; Beven and Binley, 1992; Zak and Beven, 1999; Ratto et al., 2001), although other percentiles may be used (Brazier et al., 2000). It should be stressed that these predictive uncertainty bounds simply define the upper and lower prediction limits associated with the behavioural parameter sets, and do not represent probabilistic uncertainty intervals or objective probabilities.

The GLUE-based prediction limits capture the uncertainty in model output associated with uncertainty in model parameterization. Observations falling outside the uncertainty bounds are likely the result of errors in input data, model structure and/or observed variables (Beven and Freer, 2001). The reader is referred to Beven and Binley (1992), Freer and Beven (1996), and Beven and Freer (2001) for additional details on the GLUE procedure.

2.3. Study site

The Jameson catchment (34 km^2), located in the San Rafael Mountains north of Santa Barbara, California, USA (Fig. 1), is one of the few remaining non-urbanised catchments in this region. There is a comprehensive geospatial dataset available for the study site including digital maps of fire history, vegetation type, soil type and elevation. The Mediterranean-type climate of this region is characterised by cool, wet winters and warm, dry summers. Annual average precipitation and streamflow in the Jameson catchment are 780 mm and 233 mm, respectively. Elevation ranges from 677 m at the catchment outlet to 1771 m at the highest point along the ridge. Sandy-loam soils are typically found on the steep, rugged hillslopes (average slope ~ 43%), while somewhat deeper sandy-loam and loam soils are found on gentler slopes. The combination of stands in different stages of post-fire succession with spatial variability in physical site characteristics (e.g. terrain and soils) produces a complex vegetation mosaic dominated by evergreen shrubs (chaparral) intermixed with oak woodlands, summer deciduous subshrubs (coastal sage scrub), conifer forest, and grassland (Stephenson and Calcarone, 1999).

2.4. Input data

Model grid cell size for the Jameson catchment was fixed at 270 m × 270 m. This spatial scale was selected to allow for the most accurate representation of catchment attributes without placing excessive demands on computer run time required for Monte Carlo simulations. Model predictions of streamflow were made at a daily time step and aggregated to monthly values for comparison with observed streamflow data. Observed values of monthly streamflow were obtained from the United States Geological Survey gage (#11121010) located at the catchment outlet (daily values were not available). Input time series and spatially distributed datasets are described below.

2.4.1. Time series data

Daily temperature and precipitation data from water years (October-September) 1961 to 1993 were obtained from National Climate Data Center (NCDC) gages in and around the Jameson catchment. The spatial distribution of individual precipitation events across the catchment was assumed to correspond to the spatial pattern of mean annual precipitation (MAP). Five distinct precipitation zones were identified in the study catchment based on a digital MAP map of Santa Barbara County. The ratio between MAP at the NCDC stations (located in Zone 1) and the MAP for each of the remaining four zones was calculated and used as the basis for redistributing observed (point) daily values of precipitation to each zone. A time series of daily rainfall values was generated for each zone using this approach.

The lack of measured wind speed, net radiation and relative humidity data precluded the use of the Penman equation (Penman, 1956) for calculating daily inputs of potential evapotranspiration (PE) for the study catchment. Instead, PE was estimated using the Hargreaves and Samani (1985) model (calibrated to regional conditions using potential evaporation data obtained from a nearby California Irrigation and

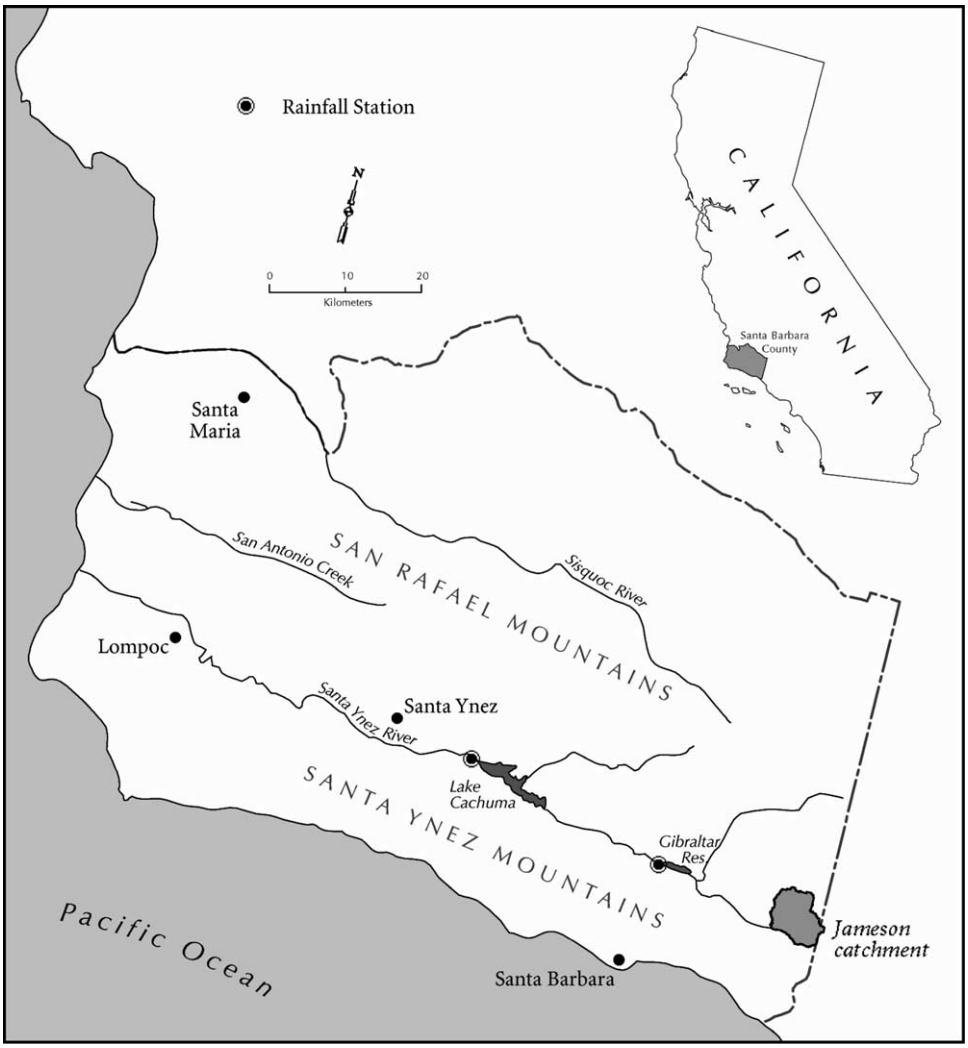

Fig. 1. The study site-Jameson catchment near Santa Barbara, California.

Management Information System (CIMIS) station) with observed (lapse-rate adjusted) daily temperature data and daily estimates of slope-aspect adjusted extraterrestrial radiation (Dingman, 1994). Spatial variation in PE across the Jameson catchment was characterised using 12 different zones, defined using three slope (low, moderate and high) and four aspect (North, East, South and West) classes. A daily time series of PE was calculated separately for each zone using the calibrated Hargreaves-Samani model.

2.4.2. Spatially distributed data

A time sequence of LAI maps was used to represent chaparral growth and recovery in MSHE_m. These maps were derived using the integrated remote sensing-chronosequence approach of McMichael et al. (2004). The basis of this approach was to convert values of the NDVI into LAI values using the generalised model of Baret et al. (1989). In this model LAI is calculated as a function of the maximum NDVI, the minimum NDVI and k, a

coefficient representing the extinction of solar radiation through the canopy. McMichael et al. (2004) used an annual time series of 10 autumn Landsat 5 Thematic Mapper (TM) and Landsat 7 Enhanced Thematic Mapper (ETM+) satellite images to derive LAI from the NDVI. Mean LAI values were recorded for a series of fires and used to derive a relationship between LAI and chaparral stand age for each image date. An average LAI-Stand Age trajectory was computed from the 10 individual relationships and used as the basis for developing input sequences of chaparral LAI for MSHE_m. While inter-annual variability in chaparral LAI was captured using this approach, intra-annual variability was not represented in the hydrological model due to: (1) the exclusive use of autumn imagery to develop the LAI-Stand Age relationships in McMichael et al. (2004), and (2) the lack of information on seasonal LAI in the chaparral literature. However, adjustments (small increases) were made to input LAI values in each of the first four years following fire (successively smaller increases each year) in order to account for the presence of herbaceous vegetation that normally occurs on post-burn chaparral sites during this period (Keeley et al., 1981; Keeley and Keeley, 1981). Input LAI sequences for non-chaparral vegetation types were derived using information from the literature (Gray and Schlesinger, 1981; Gamon et al., 1995).

Vegetation rooting depths were estimated using information from the chaparral literature (Kummerow et al., 1977; Hellmers et al., 1985) and results from a previous application of MSHE_m (using manual calibration) in the Jameson catchment (Tague et al., 2004). Existing digital vegetation, soils and elevation maps were used to delineate vegetation, soil and topographic units within the catchment. Vegetation stand age was determined by intersecting the vegetation type map (Franklin et al., 2000) with the digital fire history map. A soil profile (texture and depth of each horizon) was specified for each model grid cell using available soil survey data (3rd Order) for the study catchment (O'Hare and Hallock, 1988).

2.5. Calibration parameters

The actual number of parameters in MSHE_m depends on which modules are included in the model setup and how the catchment is discretized (horizontally and vertically). Eleven parameters were used for model calibration and uncertainty estimation in this study (see Table 1) based on previous applications of MIKE SHE (Xevi et al., 1997; Christiaens and Feyen, 2002; Vásquez et al., 2002; Vázquez and Feyen, 2003) and MSHE_m (Andersen et al., 2001; Tague et al., 2004), and the MIKE SHE user's manual (DHI Water and Environment, 2000). The range for each parameter varied in model calibration was set using previous studies and/or physical reasoning.

The parameters C_1 and C_2 control the distribution of actual evapotranspiration between transpiration and soil evaporation, while C_3 influences the value of the moisture content function (f_2). The saturated hydraulic conductivity (K_s) and exponent (n) parameters are used to compute the hydraulic conductivity as a function of effective saturation for the sandy loam (K_s_*SandyLoam* and *n_SandyLoam*) and loam (K_s_*Loam* and *n_Loam*) soil types. The remaining four parameters (IF_t, IF_h, IF_v, and GW_h) control interflow (IF) and groundwater (GW) dynamics in MSHE_m. The interflow reservoir threshold (IF_t) sets

Table 1
The initial parameter ranges used in the MSHE_m Monte Carlo simulations and the final ranges associated with the behavioural parameter sets.

Parameter	Initial Minimum Value	Initial Maximum Value	Final Minimum Value	Final Maximum Value
Interflow and Groundwater Reservoirs				
IF_t (m)	0.0001	0.3	0.0006	0.1901
IF_h (days)	0.0001	3	0.0121	3
IF_v (days)	0.0001	80	0.2085	80
GW_h (days)	0.05	100	0.08	96
Soil				
K_s_Sandy Loam (m s^{-1})	1.0×10^{-6}	5.0×10^{-4}	1.0×10^{-6}	5.0×10^{-4}
n_Sandy Loam	1	30	1	30
K_s_Loam (m s^{-1})	1.0×10^{-6}	5.0×10^{-4}	1.0×10^{-6}	5.0×10^{-4}
n_Loam	1	30	1	30
Vegetation				
C_1	0.01	1	0.13	1
C_2	0.01	1	0.01	1
C_3 (mm day^{-1})	1	60	1	60

the storage capacity of the reservoir. The horizontal time constant (IF_h) regulates interflow between reservoirs, or between a reservoir and the river, and the vertical time constant (IF_v) controls interflow contribution to groundwater. The groundwater reservoir time constant (GW_h) governs the rate of baseflow contribution to streamflow

The following assumptions were made in order to minimize the number of parameters used in model calibration. First, only the values of C_1, C_2, and C_3 for shrubland vegetation types (chaparral and coastal sage scrub) were used in calibration since more than 85% of the catchment area was classified as shrubland and it was the only vegetation type impacted by fire. Parameter values for other vegetation types were held constant. In addition, we assigned the same values of IF_t, IF_h, and IF_v to each interflow reservoir (after Andersen et al., 2001) since no information was available to guide a separate parameterisation for each reservoir.

2.6. Model calibration, testing, and uncertainty estimation

The number of Monte Carlo runs implemented in a particular GLUE-based application is a function of the interactions between catchment size, model structure (including grid cell size), the number of parameters, and the available computer resources. Tens of thousands (Zak and Beven, 1999) to millions (Brazier et al., 2000) of runs can be made when model codes are less complex, grid cell size is large, extensive computing power is available, and/or for smaller catchments. The physically-based, distributed MSHE_m model code is complex and, therefore, computer intensive. This fact, coupled with the relatively large number of grid cells required for this medium-size catchment, constrained the number of Monte Carlo simulations used in this work to 1000. Ideally more than 1000 simulations would be used in a real-world application of this model, however we felt that this number was appropriate for demonstrating our methodology for coupling MSHE_m with the GLUE procedure in the study catchment.

One thousand parameter sets, whose values were randomly selected from uniform distributions across the defined range for each parameter (see Table 1 for these 'initial' parameter ranges), were used to make Monte Carlo simulations for a 20 year calibration period (water years 1962–1981) encompassing a wide range of climatic conditions and containing one small wildfire (one percent of the catchment area, October 1971) and one medium size wildfire (20% of the catchment area, September 1964). A standard performance metric, the Nash and Sutcliffe (1970) coefficient of efficiency, E (1), was used to evaluate model performance following each run:

$$E = 1 - \frac{\sum_{j=1}^{n}(O-P)^2}{\sum_{j=1}^{n}(O-\bar{O})^2} \quad (1)$$

in which O is the observed flow, $\bar{O}$ is the mean observed flow, and P is the predicted flow. $E=1$ when all the predictions equal their corresponding observations; $E=0$ when model predictions estimate the mean observed streamflow. The coefficient of efficiency was chosen as the likelihood measure to evaluate the accuracy of both the magnitude and timing of predicted flows (e.g. Andersen et al., 2001; Beven, 2001; Vásquez et al., 2002; Tague et al., 2004). The 'behavioural' threshold value of E used in this application of MSHE_m followed Andersen et al. (2001), where good model runs were those with $E \geq 0.80$. [Note: the first two water years in each simulation run in this study were excluded from the calculation of E and from the computation of uncertainty bounds.] With a few exceptions, the final minimum and maximum parameter values for the set of behavioural model runs were similar to the initial values defined for each parameter (see Table 1 for the 'final' parameter ranges), indicating that the 1000 Monte Carlo simulations used in this study effectively sampled across the entire range of each parameter's initial distribution.

The group of behavioural parameter sets identified in the calibration period were subsequently used to make simulations for a second (test) period in order to evaluate the robustness of these behavioural sets under a range of hydrological conditions in the study catchment. The test period (water years 1982–1993) contained one very large wildfire (78% of the catchment area, July 1985) and experienced highly variable climatic conditions. Model predictions made using the behavioural parameter sets in the calibration and test periods were used to calculate the 5th and 95th percentiles (i.e. uncertainty bounds) for each

period using the GLUEWIN software package (Ratto and Saltelli, 2001); observed streamflow values from each period were compared with the corresponding uncertainty bounds.

2.7. Uncertainty in LAI inputs-effects on MSHE_m predictive uncertainty

The effects of uncertainty in LAI inputs on the uncertainty associated with MSHE_m streamflow predictions (i.e. predictive uncertainty) for the Jameson catchment were examined following model calibration and testing for the second (test) period-when inter-annual changes in canopy leaf area were most rapid due to the very large fire in 1985. Seven different model scenarios were implemented for this period, one using the baseline LAI sequence (i.e. the sequence used in the GLUE-based model calibration and testing phase of this study) and six others generated by increasing and decreasing this baseline sequence by 10, 20, and 40%. These percentage increments were selected to cover the potential range of (unknown) error levels associated with remote sensing-based estimates of LAI. Model simulations were run for each scenario using the suite of behavioural parameter sets identified during model calibration. The 90% uncertainty interval (i.e. the range of acceptable model predictions) was computed for each scenario as the range defined by the 5% and 95% uncertainty bounds. The effect of uncertainty in LAI inputs on MSHE_m predictive uncertainty was examined by comparing uncertainty intervals between each of the six scenarios and the baseline case, as well as among scenarios.

3. Results and discussion

3.1. Model calibration and testing

3.1.1. Model calibration

One hundred and nine of the 1000 Monte Carlo-based runs in the calibration period were classified as behavioural, with values of E ranging from 0.80 to 0.92. This proportion of behavioural parameter sets is comparable to that found in other GLUE-based modelling studies (e.g. Brazier et al., 2000; Beven and Freer, 2001). Predicted monthly streamflow values for each of the 109 behavioural parameter sets (excluding the first two water years) were used to compute the 5% and 95% uncertainty bounds. Approximately 68% of the observed streamflow values fell within these bounds (Fig. 2); the remaining 32% produced just over six percent of the observed streamflow total. This level of flow prediction error (i.e. $<10\%$) was considered acceptable for the

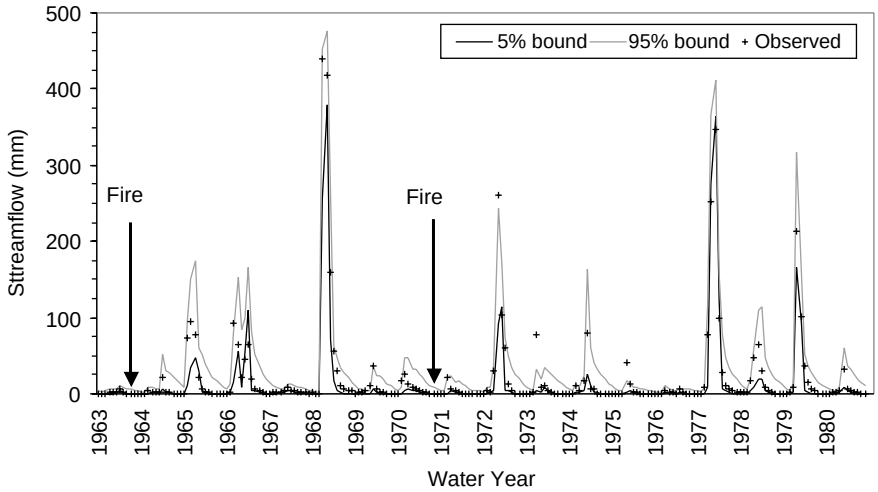

Fig. 2. The 5% and 95% uncertainty bounds with observed monthly streamflow values for the calibration period. The timing of the 1964 and 1971 wildfires are labelled in the figure.

calibration period as a whole (after Andersen et al., 2001).

Observed streamflow values in four of the 18 water years evaluated in this period were completely contained within the uncertainty bounds (Fig. 2). [Recall that model predictions from the first two years in the 20 year calibration period, and in the 12 year test period, were not considered in the calculation of E, nor in any analysis of model results.] Considering the large variability in rainfall totals for these years, ranging from low (1968 and 1981) to moderate (1979) to very high (1969), it is apparent that the group of 109 behavioural parameters sets was capable of accurately representing integrated catchment behaviour (streamflow) under different rainfall conditions in this period. However, catchment behaviour was not always so well modelled and some level of prediction error (i.e. under- and/or over-estimation) occurred in each of the remaining 14 water years in this period (results not shown).

3.1.2. Model testing

Each of the 109 behavioural parameter sets identified using data from the calibration period was used to make daily streamflow predictions for the test period in order to evaluate their robustness under different fire and rainfall regimes; daily predictions were aggregated to monthly values and used to calculate the test period uncertainty bounds. Approximately 67% of the observed streamflow values fell within the 5% and 95% uncertainty bounds (Fig. 3); the remaining 33% of observed values produced approximately nine percent of the observed streamflow total (considered acceptable for the test period as a whole).

The average range between the upper and lower uncertainty bounds (R_{avg}) was largest in wet season months (November-April, Fig. 4a), with values decreasing steadily through the transition (May-June) and dry (July-October) seasons. That is, greater predictive uncertainty was associated with high flows than with low flows. On the other hand, values of the normalized average range (NR_{avg}) (computed by dividing the uncertainty range for each time step by the observed flow depth and re-calculating R_{avg}) were largest (i.e. uncertainty was greatest) in transition and dry season months (Fig. 4b). Variability about R_{avg} and NR_{avg} was highest in wet season and dry season months, respectively, resulting from year to year differences in predictive uncertainty. Overall, these trends were very similar to those seen in the calibration period (results not shown).

In contrast to the calibration period, prediction errors were found in every year in the test period. As with predictions in the calibration period, the largest under-estimation errors (observed values above the

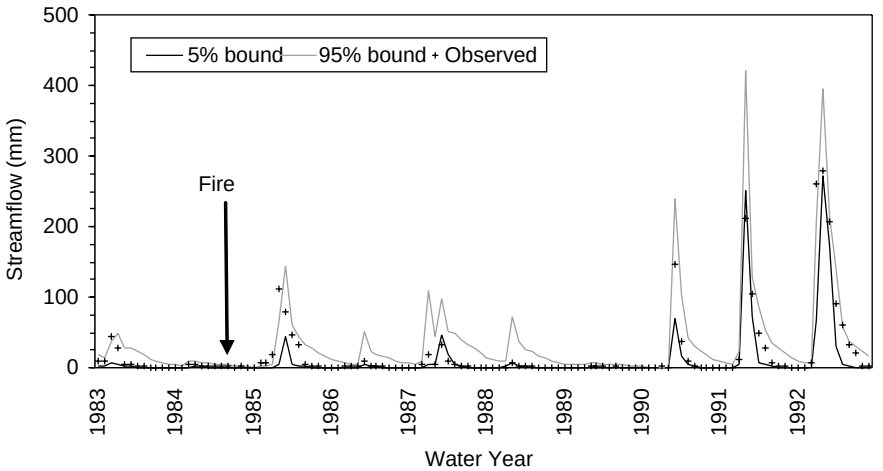

Fig. 3. The 5% and 95% uncertainty bounds with observed monthly streamflow values for the test period. The timing of the 1985 wildfire is labelled in the figure.

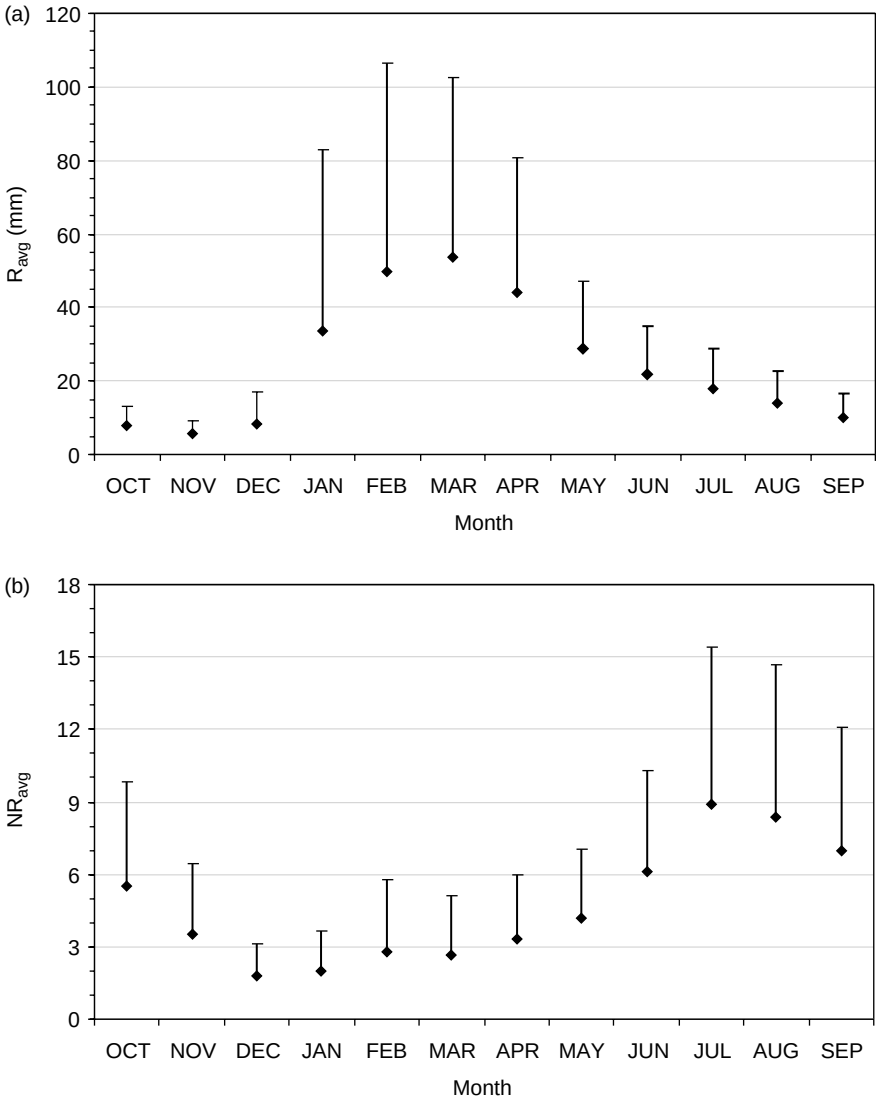

Fig. 4. The (a) average predictive uncertainty (R_{avg}), by month, and (b) R_{avg} normalized for observed streamflow (NR_{avg}), by month for the test period. One standard deviation above the mean is shown in for both figures to illustrate the variability in predictive uncertainty for each month.

95% bound) and over-estimation errors (observed values below the 5% bound) occurred in wet season months (Fig. 5). Under- and over-estimation errors in this period, as in the calibration period, were associated primarily with large events (e.g. 390 mm of rainfall over six days in 1993) in high rainfall years. In addition, a large portion of the total under-estimation error in the test period occurred in the water year following the 1985 wildfire.

3.1.3. Discussion-model calibration and testing

Virtually the same proportion of observed monthly streamflow values was captured by the 5% and 95% uncertainty bounds in the calibration and testing periods, despite different rainfall patterns and wildfire conditions. The total prediction error (i.e. the sum of over- and under-estimation errors) for each period as a whole was considered acceptable as it represented less than 10% of the observed flow. Even so, the fact that

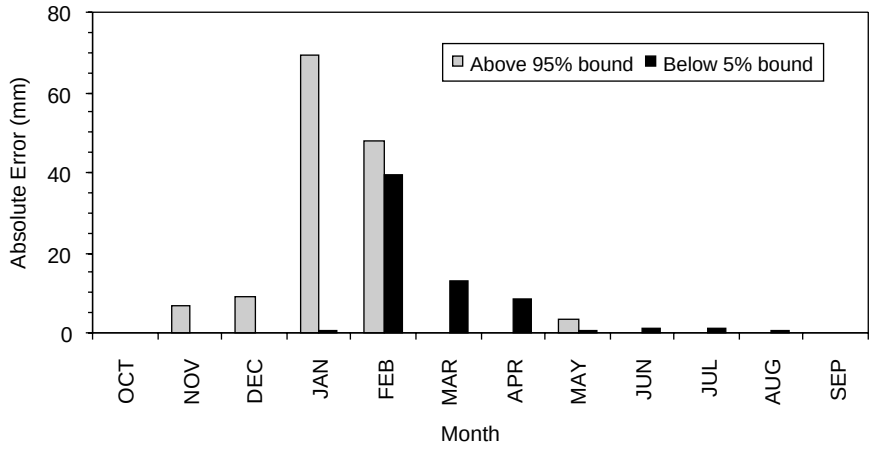

Fig. 5. The test period 'absolute error' was calculated, for each observation not contained by the uncertainty bounds, as the absolute difference between the observed value and the nearest uncertainty bound. Under-estimation occurred when observed values fell above the 95% bound; over-estimation occurred when observations fell below the 5% bound.

just over 30% of the observed streamflow values in each period fell outside of the 90% uncertainty bounds suggests an overall bias in the model's ability to estimate observed flows in the Jameson catchment, especially low flows (Fig. 6).

Seasonal trends in R_{avg} and NR_{avg} in the test period were very similar to those found in the calibration period, demonstrating a level of consistency in modelled high, moderate, and low flows across periods. Differences in the magnitude and variability of R_{avg} and NR_{avg} between the calibration and testing periods were generally small, however their respective non-Gaussian distributions further suggest a level of model bias in matching observed flows for the study catchment. Overall, average predictive uncertainty (R_{avg}) was greatest, and most variable, in wet season months, declining through the transition and dry seasons. However, the opposite pattern was seen once R_{avg} was normalized for observed flow (NR_{avg}), indicating that the mean relative predictive uncertainty was greatest in dry season months. That is, model predictions were most uncertain, relative to

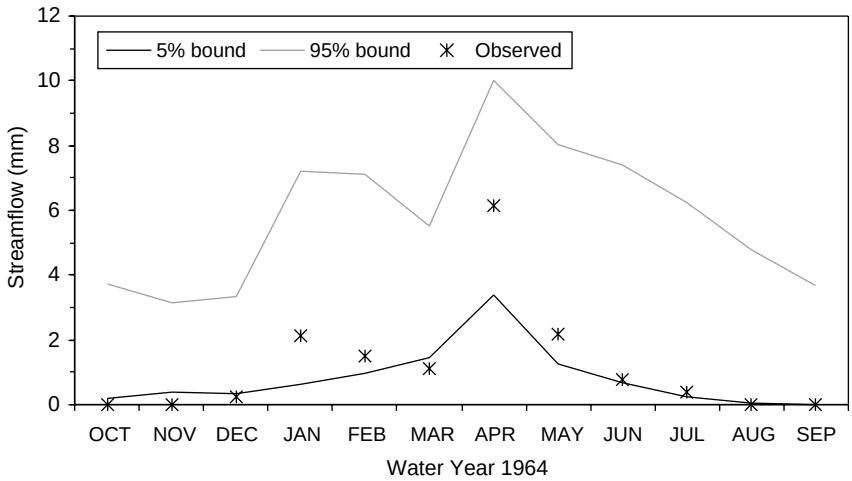

Fig. 6. Results for one water year from the calibration period (1964) illustrate the model's difficulty in estimating low flows (see Fig. 2 for results from the entire calibration period).

observed values, in months when streamflow was low to non-existent; the relative variability in predictive uncertainty was also greatest in the dry season. In wet season months NR_{avg} was generally less than 5% of the observed flow and the relative variability in predictive uncertainty was small. The fact that NR_{avg} was less than 10% of observed flow in all seasons suggests that (on average) MSHE_m predictions of monthly streamflow in this catchment were relatively certain for both evaluation periods. Even so, the wide absolute uncertainty bounds observed in many wet season months, and following the large wildfire in 1985, indicate that the group of behavioural parameter sets used in this application of MSHE_m does not represent the full range of hydrological processes in the Jameson catchment.

Over-estimation errors in dry months (July-October) represented less than 1.5% of the total prediction error in each evaluation period. Monthly streamflow was not under-estimated during the dry season in either the calibration or test period. Absolute over- and under-estimation errors in transition months (May-June) were also very small, comprising just 1% and 2.5% of the total error in the calibration and test period, respectively. Overall, total streamflow in both transition and dry months was modelled with acceptable errors by MSHE_m using the group of 109 behavioural parameter sets, indicating that the moderate and low flow conditions were generally well characterised by the model structure.

Estimation errors (over and under) were largest in wet season months (November-April), comprising 98% of the total estimation error in each evaluation period. In contrast to findings for the transition and dry seasons, catchment processes in the wet season were not always characterised adequately by MSHE_m, particularly in relation to large storms and extensive wildfire. The patterns of over- and under-estimation were notably different between wet season months in the calibration and test periods. Over- and under-estimation errors generally increased from November through April in the calibration period, while nearly the opposite pattern was seen in the test period. This phenomenon is somewhat difficult to explain given that errors in both periods were associated with large rainfall events.

Differences in under- and over-estimation errors following fire in September 1964 (20%), October 1971 (1%), and July 1985 (78%) are most likely a function of the variability in fire size. The lack of appreciable estimation error in water years 1965 (597 mm of rainfall) and 1972 (417 mm of rainfall) indicates that the GLUE-based calibration of MSHE_m successfully captured post-fire catchment behaviour over a range of fire size (1–20%) and rainfall conditions (including large storm events). On the other hand, nearly half of the total test period under-estimation error occurred in water year 1986 (830 mm of rainfall) following the massive fire in July 1985. Errors that year were largely associated with sizable rainfall events (e.g. 196 mm in three days in February 1986) in wet season months. While these errors represent only 3% of the total observed flow in the test period, they highlight deficiencies in the ability of the model structure and/or input data to fully characterise successional dynamics in this catchment following very large fires.

3.2. Effects of uncertainty in LAI inputs on MSHE_m predictive uncertainty

For ease of discussion the six LAI scenarios are labelled using either a '+' or '−', depending upon whether simulated uncertainty of 10, 20 and 40% was added to (+10, +20 and +40) or subtracted from (−10, −20 and −40) the baseline LAI sequence. The 90% uncertainty interval (UI) was calculated using predicted monthly streamflow values for each of the seven LAI sequences as the difference between the 5% and 95% uncertainty bounds (i.e. the total distance between the bounds). The relative change in the UI (UI_{rc}) between each of the six scenarios and the baseline case was calculated as: $UI_{rc} = (UI_{scenario} - UI_{baseline})/UI_{baseline}$. Positive (negative) values of UI_{rc} indicated an increase (decrease) in predictive uncertainty resulting from uncertainty in the LAI inputs.

The relative change in MSHE_m predictive uncertainty (UI_{rc}) associated with each uncertainty scenario is shown in Fig. 7. Overall, the amount of uncertainty associated with monthly streamflow predictions increased when input LAI was lowered below the baseline (−10, −20 and −40 scenarios), while predictive uncertainty decreased for LAI inputs above the baseline sequence (+10, +20 and +40 scenarios). Values of UI_{rc} generally followed the

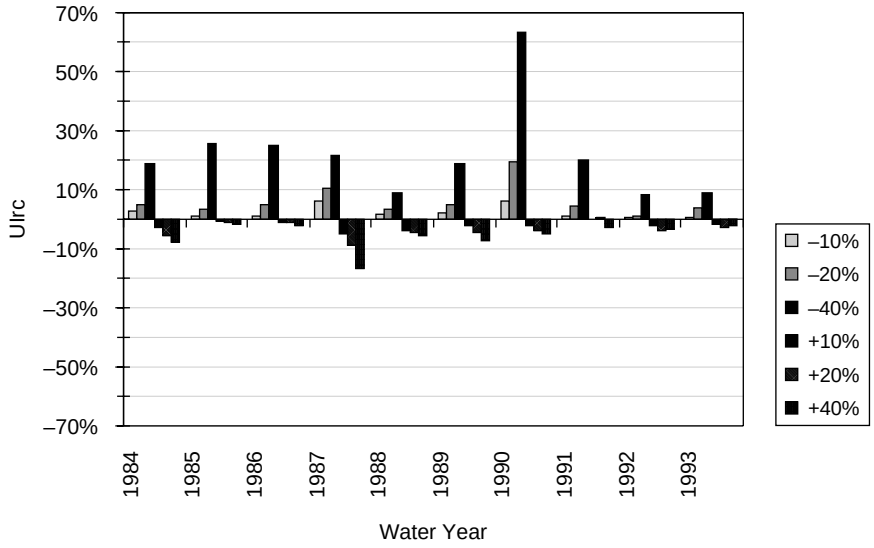

Fig. 7. Relative changes in predictive uncertainty (UI_{rc}) for each LAI uncertainty scenario over the test period.

expected directional trends, with values becoming progressively larger as input errors progressed from ± 10 to 40%. The largest values of UI_{rc} over the post-fire recovery period (1986–1993) occurred for LAI inputs below the baseline, especially with the -40 uncertainty scenario. Values of UI_{rc} were less than 10% for the -10, $-20, +10$ and $+20$ uncertainty scenarios over this period, with the exception of the -20 scenario in 1987 and 1990 (two very dry years).

Values of UI_{rc} associated with the $+10, +20$ and $+40$ uncertainty scenarios were much smaller than values related to the -10, -20 and -40 scenarios in the first year following fire (1986, Fig. 7). LAI inputs above the baseline had little effect on values of UI_{rc} in 1986, suggesting that the baseline sequence may represent an 'LAI asymptote' for this catchment condition (i.e. first post-fire year). However, this finding could also be the result of over-estimating the baseline LAI input immediately following fire, in which case further additions to input LAI would not substantially alter model streamflow predictions. In contrast, lowering input LAI below the baseline resulted in higher predicted flows and larger values of UI_{rc}.

Modified LAI inputs in the second post-fire year (1987) produced proportional changes in predictive uncertainty for the ± 10, 20 and 40% scenarios (Fig. 7). Moreover, UI_{rc} values for this year were generally much larger than in 1986, possibly due to the extremely dry conditions in 1987 (272 mm). This result implies that streamflow dynamics may be very sensitive to canopy leaf area in dry years. Raising LAI above the baseline in 1987 reduced predicted streamflow values and narrowed the uncertainty bounds (i.e. reduced predictive uncertainty). In contrast, predictive uncertainty increased when input LAI was below the baseline sequence by even a small percentage. Raising LAI inputs above the baseline had an increasingly smaller effect on UI_{rc} values in the third through eighth post-fire years (Fig. 7). This may be explained, at least in part, by the formulation of the transpiration function $f_1(LAI)$ in MSHE_m which tends to limit the effect of increasing LAI after a threshold value determined by the C_1 and C_2 parameters. The effects of reducing LAI inputs below the baseline during this period varied with rainfall conditions and were generally largest in drier years.

Values of UI_{rc} were highest in wet season months (November-April), decreasing into the transition (May-June) and dry (July-October) season months (Fig. 8). UI_{rc} values associated with the ± 10 and 20% uncertainty scenarios were less than 10% in all months, as were values corresponding to the $+40$ scenario. However, values UI_{rc} for the -40 scenario

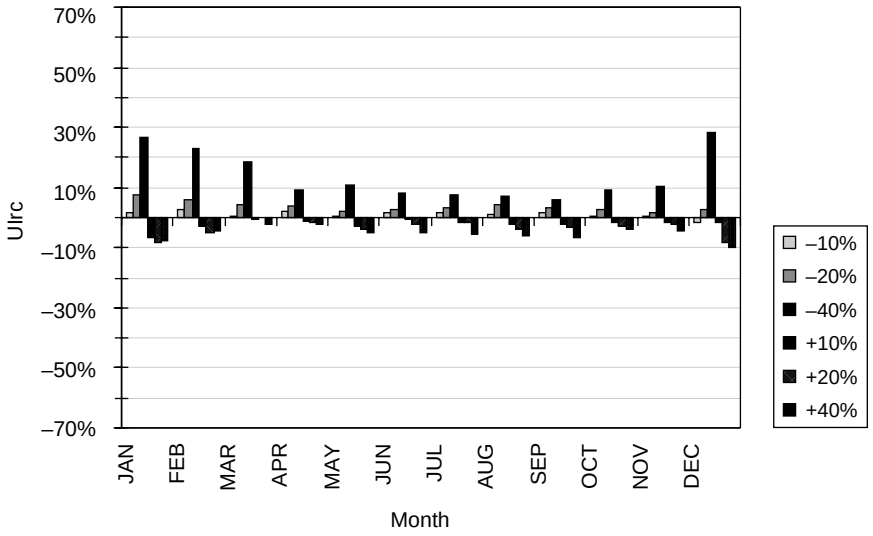

Fig. 8. Relative changes in predictive uncertainty (UI_{rc}) for each LAI uncertainty scenario over the test period-by month.

were greater than 10% in six of twelve months, including all wet season months except April. Overall, uncertainty in LAI inputs had the greatest impact on catchment water balance in wet season months as canopy leaf area directly affects the partitioning of rainfall into evapotranspiration and streamflow in MSHE_m. The potential under-estimation of input LAI values in the growing season (due to the exclusive use of autumn imagery by McMichael et al., 2004) may also have contributed to greater relative predictive uncertainty in these months.

3.3. Additional sources of uncertainty and error

3.3.1. Model structure

The general lack of information and data for subsurface conditions in the study catchment precluded the use of the 3-D groundwater module available in the full version of MIKE SHE. Instead, we implemented the semi-distributed Linear Reservoir groundwater module with three interflow reservoirs and one ground water reservoir (MSHE_m). The Linear Reservoir module does not allow interactions and feedback between the saturated and unsaturated zones and, consequently, may not adequately represent subsurface flow dynamics under all conditions. Moreover, MSHE_m is not capable of representing time-varying soil properties. This may be an important limitation of the model as fire has been shown to alter soil physical properties in California chaparral ecosystems (DeBano and Conrad, 1978), potentially modifying soil water-holding capacity.

The grid cell size used in this study (270 m × 270 m) may be considered somewhat coarse given the rugged nature of the terrain in the study area. However, results from previous studies using MIKE SHE and MSHE_m demonstrate that overall model performance is marginally sensitive to changes in grid cell size for small (1 km^2, MIKE SHE, Xevi et al., 1997), medium (34 km^2, MSHE_m, Tague et al., 2004), and large catchments (568 km^2, MIKE SHE, Vásquez et al., 2002). For example, Vásquez et al. (2002) found little change in a number of model performance measures when MIKE SHE was applied over a range of grid cell sizes (300–1200 m) in a large catchment. The manual calibration and application of MSHE_m at 30 m and 270 m grid cell resolutions in the Jameson catchment resulted in very similar values of E, 0.96 and 0.93 respectively, when comparing monthly streamflow predictions with observed data (Tague et al., 2004).

Previous work has demonstrated that the identification of behavioural parameter sets is directly influenced by the choice of likelihood measure and/or the corresponding threshold value (Beven and Binley, 1992; Freer and Beven, 1996). In this study 109

Table 2
The relationships between likelihood measures, behavioural threshold values, and the number of behavioural parameter sets

Likelihood Measure	Threshold = 0.50	Threshold = 0.60	Threshold = 0.70	Threshold = 0.80
E[a]	609[b]	440	238	109
lnE[c]	189	122	74	16

[a] E is the coefficient of efficiency (see Section 2.6 for calculation).
[b] The number of behavioural parameter sets resulting from a specific likelihood measure-behavioural threshold combination.
[c] lnE was calculated by taking the natural log of observed and predicted streamflow values prior to computing the coefficient of efficiency, E.

parameter sets out of 1000 were classified as behavioural based on a 0.80 threshold of the coefficient of efficiency. As stated earlier this proportion of behavioural parameter sets is similar to that reported in other GLUE-based studies, however the absolute number of behavioural sets identified in this study is much smaller. A larger number of Monte Carlo simulations (e.g. 10,000) would likely yield additional behavioural parameter sets and provide a more thorough sampling of the parameter space. However, a substantial increase in computing resources would be required to make this number of runs for such a complex model.

The number of behavioural parameter sets used to calculate the 5% and 95% predictive uncertainty bounds might also be increased by selecting a different likelihood measure and/or threshold value during the GLUE procedure. For instance, reducing the selected threshold value for the coefficient of efficiency (E) would have increased the number of behavioural parameter sets utilized in this study (Table 2). Moreover, using a different likelihood measure and/or behavioural threshold would have altered not only the *number* of behavioural parameter sets selected (Table 2), but the *particular* parameter sets selected from the group of 1000 Monte Carlo simulations. From these results it could be expected that the proportion of observations falling within the 90% uncertainty interval would continue to grow as the number of behavioural parameter sets increased and the range between the 5% and 95% uncertainty bounds widened. However, Hope et al. (2004) demonstrated that this expectation may not always be correct via a GLUE-based application of the HSPF (Hydrologic Simulation Program Fortran) model in the same study catchment (Jameson). Specifically, they found that the number of observations falling within the 90% uncertainty interval remained fairly constant as the E threshold was lowered from 0.80 to 0.60, even though a much larger number of behavioural parameter sets was identified using the 0.60 threshold value. Further reductions in the E threshold from 0.60 to 0.40 actually resulted in a *decrease* in the number of observations captured between the 5% and 95% uncertainty bounds.

3.3.2. Model inputs and observed data

Errors and uncertainty associated with model inputs (in addition to LAI) and observed data may also have contributed to predictive uncertainty and prediction errors in this study. For example, given the generally rugged nature of the study catchment, there is uncertainty associated with the assumption that the spatial distribution of rainfall for individual events in Jameson followed the mapped pattern of mean annual precipitation for this area. Consequently, it is possible that the number of precipitation zones used in this study (five) did not adequately prescribe input rainfall values for Jameson. In addition, uncertainty in input PE values may have resulted from calibrating the Hargreave-Samani PE model using data from a neighbouring area, as well as from subdividing the study catchment into twelve PE zones by classifying continuous surfaces (slope and aspect) into discrete units. Finally, it is expected that errors associated with observed data used in developing and characterising model inputs (e.g. daily rainfall and temperature data, and soil survey data) and outputs (monthly streamflow data) were propagated through the current model application.

4. Conclusions

Results from the GLUE-based calibration and testing of MSHE_m provide insights into both the strengths and weaknesses of the combined model structure, parameters and input data as a tool for predicting integrated catchment behaviour in the Jameson catchment.

Overall, model performance in the calibration period was somewhat better than in the test period. Approximately two-thirds of the observations (comprising over 90% of the total observed flow) in each period were contained within the uncertainty bounds, an acceptable level of model performance relative to total period flow. However, the fact that the greatest prediction errors were associated with critical catchment events, i.e. large storms and large wildfires, suggests that refinements are needed to improve MSHE_m performance and reduce predictive uncertainty at the monthly/seasonal time scales.

Examination of the effects of uncertainty in LAI inputs on MSHE_m predictive uncertainty revealed little difference (generally less than 10%) between the 'baseline' LAI sequence and the six 'LAI uncertainty scenarios' for the test period. This finding indicates that the remote sensing-based LAI estimates used in this study are generally appropriate for distributed hydrological modelling in this environment. Nevertheless, given that some of the largest differences in predictive uncertainty were observed in the first few years following fire, particularly in wet season months, future work will focus on refining both inter- and intra-annual LAI estimates for this initial recovery period. Additional sources of uncertainty and error discussed above will be investigated in future work (e.g. spatially distributed rainfall inputs).

GLUE provides a useful modelling approach for advancing beyond globally optimised, unique, parameter sets. Working within a framework of Monte Carlo-generated parameter sets allows modellers to explicitly recognize and quantify the effects of uncertainties on model predictions. Future versions of commercially available hydrological modelling systems should incorporate the flexibility to conduct GLUE-based modelling and uncertainty estimation-particularly given the use of distributed model predictions as a basis for environmental decision-making.

Acknowledgements

Funding for this research was provided in part by a NASA Land Use Land Cover Change Grant (No. NAG5-11141), a NASA Earth System Science Fellowship (No. NGT5-30335), and a NSF Doctoral Dissertation Research Improvement Grant (No. BCS-0000233).

The authors would like to thank: Drs. Dar Roberts and Janet Franklin for their insightful comments on this manuscript; Drs. Joel Michaelsen and Max Moritz, David McKinsey, Jon Ahlroth, Matthew Naftaly, Ken Oster and Bill Ferguson for help with dataset compilation; Torsten Jacobsen, Henrik Sorensen, Henrik Madsen, Thomas Clausen, Birgitte von Christierson, and Oluf Jessen of the Danish Hydraulic Institute for MIKE SHE technical support; Michael Anaya, Robyn Clark, W. Casey McMichael and Jared Aldstadt for assistance with data processing; and Harry Johnson for designing the study site map. Useful comments from two reviewers are also appreciated.

References

Abbott, M.B., Bathurst, J.A., Cunge, P.E., O'Connell, J., Rasmussen, J., 1986a. An introduction to the European Hydrological System - Système Hydrologique Européen'SHE 1: history and philosophy of a physically based distributed modelling system. Journal of Hydrology 87, 45–59.

Abbott, M.B., Bathurst, J.A., Cunge, P.E., O'Connell, J., Rasmussen, J., 1986b. An introduction to the European hydrological system—Système hydrologique Européen 'SHE' 2: structure of a physically based distributed modelling system. Journal of Hydrology 87, 61–77.

Andersen, J., Refsgaard, J.C., Jensen, K.H., 2001. Distributed hydrological modelling of the Senegal River Catchment—model construction and validation. Journal of Hydrology 247, 200–214.

Andersen, J., Dybkjaer, G., Jensen, K.H., Refsgaard, J.C., Rasmussen, K., 2002. Use of remotely sensed precipitation and leaf area index in a distributed hydrological model. Journal of Hydrology 264, 34–50.

Baret, F., Olioso, A., Luciani, J.L., Hanocq, J.F., 1989. Estimation de l'énergie photosynthétiquement active absorbée par une culture de blé à partir de données radiométriques. Agronomie 9, 885–895.

Beven, K.J., 2001. Rainfall-Runoff Modelling: the Primer. Wiley, West Sussex, England, p. 360.

Beven, K., Binley, A., 1992. The future of distributed models: model calibration and uncertainty prediction. Hydrological Processes 6, 279–298.

Beven, K., Freer, J., 2001. Equifinality, data assimilation, and uncertainty estimation in mechanistic modelling of complex environmental systems using the GLUE methodology. Journal of Hydrology 249, 11–29.

Binley, A.M., Beven, K.J., 1991. Physically-based modelling of catchment hydrology: a likelihood approach to reducing

predictive uncertainty. In: Farmer, D.G., Rycroft, M.J. (Eds.), Computer Modelling in the Environmental Sciences. Clarendon Press, Oxford, pp. 75–88.

Brazier, R.E., Beven, K.J., Freer, J., Rowan, J.S., 2000. Equifinality and uncertainty in physically based soil erosion models: an application of the GLUE methodology to WEPP— the water erosion prediction project—for sites in the UK and USA. Earth Surface Processes and Landforms 25, 825–845.

Christiaens, K., Feyen, J., 2002. Constraining soil hydraulic parameter and output uncertainty of the distributed hydrological MIKE SHE model using the GLUE framework. Hydrological Processes 16, 373–391.

Davis, F.W., Michaelsen, J., 1995. Sensitivity of fire regime in chaparral ecosystems to global climate change. In: Oechel, W. C., Moreno, J.M. (Eds.), Global Change and Mediterranean-Type Ecosystems. Springer, New York, pp. 435–456.

DeBano, L.F., Conrad, C., 1978. The effect of fire on nutrients in a chaparral ecosystem. Ecology 59, 489–497.

DHI Water and Environment, 2000.Anon., 2000. MIKE SHE: Pre- and Post-processing User Manual 2000.

Dingman, S.L., 1994. Physical Hydrology. Prentice Hall, Englewood Cliffs, NJ pp. 575.

Franklin, J., Woodcock, C.E., Warbington, R., 2000. Digital vegetation maps of forest lands in California: integrating satellite imagery, GIS modelling, and field data in support of resource management. Photogrammetric Engineering and Remote Sensing 66, 1209–1217.

Freer, J., Beven, K., 1996. Bayesian estimation of uncertainty in runoff prediction and the value of data: an application of the GLUE approach. Water Resources Research 32, 2161–2173.

Gamon, J.A., Field, C.B., Goulden, M.L., Griffin, K.L., Hartley, A. E., Joel, G., Penuelas, J., Valentini, R., 1995. Relationships between NDVI, canopy structure, and photosynthesis in three Californian vegetation types. Ecological Applications 5, 28–41.

Gray, J.T., Schlesinger, W.H., 1981. Biomass, production and litterfall in the coastal sage scrub of southern California. American Journal of Botany 68, 24–33.

Hargreaves, G.H., Samani, Z.A., 1985. Reference crop evapotranspiration from temperature. Applied Engineering in Agriculture 1, 96–99.

Hellmers, H., Horton, J.S., Juhren, G., O'Keefe, J., 1985. Root systems of some chaparral plants in southern California. Ecology 36, 667–678.

Hope, A.S., Stein, A.K., McMichael, C.E., 2004. Uncertainty in monthly river discharge predictions in a semi-arid shrubland catchment. Hydrology: Science & Practice for the 21st Century. British Hydrological Society, Dundee, Scotland, pp. 284–290.

Hoyt, W.G., Troxell, H.C., 1932. Forests and streamflow. Proceedings of the American Society of Civil Engineers 58, 1037–1066.

Keeley, J.E., Keeley, S.C., 1981. Post-fire regeneration of southern California chaparral. American Journal of Botany 68, 524–530.

Keeley, S.C., Keeley, J.E., Hutchinson, S.M., Johnson, A.W., 1981. Post-fire succession of the herbaceous flora in southern California chaparral. Ecology 62, 1608–1621.

Kummerow, J., Krause, D., Jow, W., 1977. Root systems of chaparral shrubs. Oecologia 29, 163–177.

Kristensen, K.J., Jensen, S.E., 1975. A model for estimating actual evapotranspiration from potential evapotranspiration. Nordic Hydrology 6, 170–188.

Lavabre, J., Sempere Torres, D., Cernesson, F., 1993. Changes in the hydrological response of a small Mediterranean catchment a year after a wildfire. Journal of Hydrology 142, 273–299.

Lenihan, J.M., Drapek, R., Bachelet, D., Neilson, R.P., 2003. Climate change effects on vegetation distribution, carbon and fire in California. Ecological Applications 13, 1667–1681.

Loaiciga, H.A., 2003. Hydrologic-hydraulic calibration and testing in an impacted flood plain: forensic hydrology. Calibration of Watershed Models: Water Science and Application 6. American Geophysical Union, Washington D.C, pp. 175–184.

Loaiciga, H.A., Marino, M.A., 1987. Parameter estimation in groundwater: classical, Bayesian, and deterministic assumptions and their impact on management policies. Water Resources Research 23, 1027–1035.

Loaiciga, H.A., Pedreros, D., Roberts, D., 2001. Wildfire-streamflow interactions in a chaparral Catchment. Advances in Environmental Research 5, 295–305.

Mackay, D.S., Band, L.E., 1997. Forest ecosystem processes at the watershed scale: dynamic coupling of distributed hydrology and canopy growth. Hydrological Processes 70, 1197–1217.

McMichael, C.E., Hope, A.S., Roberts, D.A., Anaya, M.R., 2004. Post-fire recovery of leaf area index in California chaparral: a remote sensing-chronosequence approach. International Journal of Remote Sensing 25, 4743–4760.

Nash, I.E., Sutcliffe, I.V., 1970. River flow forecasting through conceptual models I. Journal of Hydrology 10, 282–290.

O'Hare, J.P., Hallock, B.G., 1988. Soil Survey of the Los Padres National Forest Area, California. United States Department of AgricultureUniversity of California, California. 148 pp..

Penman, H.L., 1956. Evaporation: an introductory survey. Netherlands Journal of Agricultural Science 4, 7–29.

Poole, D.K., Roberts, S.W., Miller, P.C., 1981. Water utilization. In: Miller, P.C. (Ed.), Resource Use by Chaparral and Matorral: A Comparison of Vegetation Function in Two Mediterranean-type Ecosystems Ecological Studies No. 39. Springer, Berlin, pp. 123–149.

Ratto, M., Saltelli, A., 2001. IMPACT Deliverable 18: Model Assessment in Integrated Procedures for Environmental Impact Evaluation—Software Prototypes. Joint Research Centre of European Commission. http://webfarm.jrc.cec.eu.int.

Refsgaard, J.C., Storm, B., 1995. MIKE SHE. In: Miller, P.C. (Ed.), Computer Models of Catchment Hydrology. Water Resources Publications, Colorado, USA, pp. 809–846.

Ryan, K.C., 1991. Vegetation and wildland fire: implications of global climate change. Environment International 17, 169–178.

Sandholt, I., Andersen, J., Dybkjær, G., Lo, M., Rasmussen, K., Refsgaard, J.C., Høgh-Jensen, K., 1999. Use of remote sensing data in distributed hydrological models: applications in the Senegal River basin. Danish Journal of Geography 99, 47–57.

Scott, D.F., 1993. The hydrological effects of fire in South African mountain catchments. Journal of Hydrology 150, 409–432.

Stephenson, J.R., Calcarone, G.M., 1999. Southern California mountains and foothills assessment: habitat and species

conservation issues. General Technical Report GTR-PSW-172. Pacific Southwest Research Station, Forest Service, US Department of Agriculture.

Tague, C., McMichael, C., Hope, A., Choate, J., 2004. Application of the RHESSys model to a California semi-arid shrubland catchment. Journal of the American Water Resources Association 40, 575–589.

Vázquez, R.F., Feyen, J., 2003. Effect of potential evapotranspiration estimates on effective parameters and performance of MIKE SHE-code applied to a medium-size catchment. Journal of Hydrology 270, 309–327.

Vásquez, R.F., Feyen, L., Feyen, J., Refsgaard, J.C., 2002. Effect of grid size on effective parameters and model performance of the MIKE SHE code. Hydrological Processes 16, 355–372.

Watson, F.G.R., Vertessy, R.A., Grayson, R.B., 1999. Large scale modelling of forest hydrological processes and their long term effect on water yield. Hydrological Processes 13, 689–700.

Xevi, E., Christiaens, K., Espino, A., Sewnandan, W., Mallants, D., Sorensen, H., Feyen, J., 1997. Calibration, validation and sensitivity analysis of the MIKE SHE model using Neuenkirchen catchment as case study. Water Resources Management 11, 219–242.

Zak, S.K., Beven, K.J., 1999. Equifinality, sensitivity and predictive uncertainty in the estimation of critical loads. The Science of the Total Environment 236, 191–214.